An Analytical Model of Heating Errors in Marine Air Temperatures from Ships

DAVID I. BERRY, ELIZABETH C. KENT, AND PETER K. TAYLOR

Southampton Oceanography Centre, Southampton, United Kingdom

(Manuscript received 3 July 2003, in final form 13 January 2004)

ABSTRACT

Marine air temperature reports from ships can contain significant biases due to the solar heating of the instruments and their surroundings. However, there have been very few attempts to derive corrections. The biases can reverse the sign of the measured air–sea temperature differences and cause significant errors in the sea surface latent and sensible heat flux estimates. In this paper a new correction for the radiative heating errors is presented. The correction is based on the analytical solution of the heat budget for an idealized ship, using empirical coefficients to represent the physical parameters. For the first time heat storage is included in the correction model. The heating errors are estimated for the Ocean Weather Ship *Cumulus* and the coefficients determined. When the correction is applied to the *Cumulus* data the average estimated error is reduced from 0.32° to 0.04°C and the diurnal cycle in the error is removed. The rms error is reduced by 30%. The correction technique, although not the coefficients derived here that are specific to the *Cumulus*, can be applied to air temperature data from any type of ship, or to data from groups of ships such as the Voluntary Observing Ships.

1. Introduction

Observations of the surface meteorological parameters by merchant ships participating in the Voluntary Observing Ships (VOS) Program are an important part of the climate record. These observations are frequently used in studies of climate change (e.g., Folland et al. 1984; Fu et al. 1999), in constructing climatologies (e.g., Rayner et al. 2003), in compiling atlases of surface heat and momentum fluxes (e.g., da Silva et al. 1994; Josey et al. 1999), in validating satellite parameters (e.g., Reynolds and Smith 1994), and for model output validation (Josey et al. 2001). The observations have also been collated in the International Comprehensive Ocean Atmosphere Data Set (ICOADS; Woodruff et al. 1998; Diaz et al. 2002). However, while these observations have been widely used, they do contain systematic and random errors and therefore need to be analyzed with care. Marine air temperature (MAT) observations are particularly prone to large systematic biases due to the solar heating of the instruments and ship's environment (e.g., Glahn 1933; Deitrich 1950; Folland 1971; Hayashi 1974; Goerss and Duchon 1980; Kent et al. 1993a). As a result of these errors, some studies use only nighttime MAT (NMAT; e.g., Smith and Reynolds 2002) or use the SST as a proxy for MAT (e.g., Trenberth et al. 1992; Parker et al. 1994; Fu et al. 1999).

Corresponding author address: David I. Berry, Southampton Oceanography Centre, European Way, Southampton SO1 43ZH, United Kingdom.
E-mail: dyb@soc.soton.ac.uk

The errors in MAT can be larger than the air–sea temperature difference, leading to an apparent reversal in sign of the implied sensible heat flux and unrealistic direct heat gain by the ocean. In addition evaporative heat loss by the ocean will be underestimated as atmospheric conditions may appear to be stably stratified rather than near neutral or unstable. For calculation of surface fluxes to 10 W m^{-2} it is necessary to know the mean air temperature to better than ± 0.2°C (Taylor et al. 2000). The radiative heating biases in VOS air temperature can be much larger than this target accuracy, implying that accurate turbulent fluxes cannot be calculated from VOS daytime air temperatures as reported. In many regions and periods VOS observations are scarce, so the recovery of daytime MAT through correction for heating errors is extremely desirable.

It should be noted that, although air temperature measurements are affected by solar radiation, the humidity remains unaffected as the ship is not usually a source or sink of moisture. If a wet- and dry-bulb psychrometer is used, the dewpoint should be calculated using the measured air temperature rather than the corrected air temperature (Kent and Taylor 1996). There may, however, be a correlation between errors in humidity and temperature as poorly ventilated sensors will give elevated estimates of both quantities (due to an underestimate of the wet-bulb depression).

A correction methodology for heating errors in nineteenth century MAT observations from individual ships has been proposed by Chenoweth (2000), and the heating errors in more recent observations have been examined and quantitatively assessed by Kent et al.

(1993b, hereafter KTT). KTT examined the differences between MAT observations and the output of a numerical weather prediction model as part of the VOS Special Observing Project for the North Atlantic (VSOP-NA; Kent et al. 1993a). They related differences between ship observations of the MAT and model output to the incident solar radiation and relative wind speed at the time of observation and proposed a correction based on these parameters. The correction of KTT works well when averaged over the VSOP-NA dataset; however, the diurnal cycle of the corrected MAT is poor. There is an overcorrection in the morning and undercorrection in the afternoon as the correction does not allow for a storage of heat by the ship, which can be significant (A. Dai 2002, personal communication).

In addition to heating errors in ship MAT observations, there are heating errors present in observations of MAT made by buoys. These have been examined by Anderson and Baumgartner (1998, hereafter AB) and a correction developed for individual buoy types. Anderson and Baumgartner model the heat budget for individual buoys, assuming a steady state and that the convective and conductive cooling balances the heating by the solar radiation. The correction of AB works well for buoys; however, it is unsuitable for ship observations of MAT as there is no allowance for the storage of heat. In this paper we develop a new correction for radiative heating errors in ship-based MAT observations by extending the model of AB to allow for storage of heat by the sensor environment. Due to the nature of the VOS, with some ships reporting infrequently, it is not always possible to determine the heating history of a ship over the course of a day. The model must therefore apply to individual ship reports where we have no knowledge of the environmental conditions prior to the observations. The heat budget is solved analytically for a simplified ship model (section 2) using parameterizations for the shortwave and longwave radiation and for the convective and conductive heat exchange. Only instantaneous values are required as input, the time-varying history of solar radiation being estimated. Empirical coefficients in the resulting model are derived using a randomly chosen subset of hourly meteorological observations from the Ocean Weather Ship *Cumulus* (section 3). The results of applying the correction model to a second independent subset of the *Cumulus* data are presented in section 4, with a discussion and conclusions in section 5. In a further study (D. I. Berry et al. 2004, unpublished manuscript), the correction model developed in this paper will be applied to VOS meteorological reports.

2. Development of the heating model

a. Introduction

In this study radiative heating errors in MAT have been modeled using the principle of conservation of energy: a heat budget approach. Convective and conductive cooling are modeled following AB, but we extend their model in several ways. We have allowed for storage of heat by the sensor environment. In this paper we use the term ''sensor environment'' to mean that part of the ship whose temperature affects the MAT. This will be the section of the ship's superstructure over which air flows before reaching the sensor, typically the bridge and accommodation block, and the part of the deck and any structures near the sensor. Anderson and Baumgartner used instantaneous values of measured solar radiation in their model. We do not do this for two reasons: first, neither the OWS *Cumulus* nor the VOS measure solar radiation and, second, to allow for heat storage we need the time history of solar radiation that is not available for VOS reports. However, if we parameterize the solar radiation using the cloud cover, we can assume the cloud cover remains constant and estimate the resulting diurnal variation in solar radiation. The AB model is further extended by including the effects of longwave radiation.

Although in this paper we test the model using observations from a single ship, the OWS *Cumulus*, we have developed the model with the aim of correcting the MAT observations from a large number of ships in the VOS fleet. We do not therefore wish to model specific details of the structure and properties of an individual ship. Rather, we shall approximate the ship as a simple homogenous block and empirically determine the thermal and physical properties by fitting the model coefficients to estimates of the heating errors and environmental conditions.

b. The heat budget

In order to model the error in MAT using a heat budget approach we need to assume that any heating of air as it flows around the ship is proportional to the heating of the sensor environment. This allows us to use the heating of the sensor environment as a measurement of the heating of the air itself, and hence the heating errors. Allowing the energy stored by the sensor environment and sensors to vary with time, the heat budget can be expressed as

$$\frac{dQ_{\text{ship}}}{dt} = Q_{\text{SW}} + Q_{\text{LW}} + Q_{\text{CONV}} + Q_{\text{COND}}, \qquad (1)$$

where Q_{ship} is the energy stored by the sensor environment and sensors (J), Q_{SW} is the rate of solar energy absorbed (W), Q_{LW} is the net rate of thermal heating and cooling (W), Q_{CONV} is the rate of energy transfer between the ship and the atmosphere through convection (W), Q_{COND} is the rate of energy transfer between the ship and the atmosphere through conduction (W), and t is time (s). We have assumed that the region of the ship influencing the MAT measurements (the sensor environment) is remote from the ocean and therefore that

TABLE 1. Coefficients for the Okta model (Dobson and Smith 1988).

Cloud cover (oktas)	a_i	b_i
0	0.400	0.386
1	0.517	0.317
2	0.474	0.381
3	0.421	0.413
4	0.380	0.468
5	0.350	0.457
6	0.304	0.438
7	0.230	0.384
8	0.106	0.285

the transfer of energy between this region and the ocean is negligible.

In this study, we wish to know the temperature of our system (i.e., the true air temperature plus the heating error) rather than the energy stored. To convert the energy stored to temperature we use

$$Q_{\text{ship}} = mcT_{\text{ship}},$$

where T_{ship} is the temperature of the sensor environment (K), m is the mass of the sensor environment (kg), and c is the specific heat capacity (J kg^{-1} K^{-1}). Hence Eq. (1) becomes

$$mc\frac{dT_{\text{ship}}}{dt} = Q_{\text{SW}} + Q_{\text{LW}} + Q_{\text{CONV}} + Q_{\text{COND}}. \quad (2)$$

Before we can solve Eq. (2), we need to parameterize the radiative (Q_{SW} and Q_{LW}) and convective and conductive components (Q_{COND} and Q_{CONV}) of the heat budget. The mass and specific heat capacity will be incorporated into the empirically determined coefficients.

c. Radiative components

1) SOLAR HEATING (Q_{SW})

The energy absorbed from the solar radiation by a surface is proportional to the amount of solar radiation and the area of the surface normal to the solar radiation [Eq. (3)]:

$$Q_{\text{SW}} = \alpha_S A_S R_S, \quad (3)$$

where α_S is solar absorptivity of the sensor environment, A_S is the area normal to the solar radiation (m^2), and R_S is the incident solar radiation (W m^{-2}). As the incident solar radiation is not usually directly measured, a parameterization based on the cloud and weather conditions is used. We have used the okta model of Dobson and Smith (1988), which parameterizes the incident solar radiation using

$$R_S = R_{\text{top}}(a_i + b_i \sin\theta)\sin\theta, \quad (4)$$

where $\sin\theta$ is the sine of solar elevation, a_i and b_i are constants fitted to the total cloud cover categories by Dobson and Smith (1988, see Table 1), and R_{top} is the solar radiation at the top of the atmosphere (1368 W m^{-2}).

While we have a time series of observations for the OWS *Cumulus* and other research ships, we wish to develop the model with the aim of correcting as many observations as possible, including VOS reports. Thus we have developed the correction using only the information available at the time of observation. Thus we assume that the integrated solar heating since sunrise is that which would have occurred at the observation position if the cloud and weather conditions had remained constant. We exclude any observations for which the weather codes indicate rain. Precipitation has not been included in the model, but we expect errors due to solar radiation to be small when it is raining and therefore leave air temperatures uncorrected. If the code indicates precipitation in the past but not at the current time, this violates the assumption of constant conditions and the air temperatures are discarded. Using the okta model with these approximations and assumptions, the solar radiation heating term becomes

$$Q_{\text{SW}} = \alpha_S A_S R_{\text{top}}(a_i + b_i \sin\theta)\sin\theta. \quad (5)$$

There are shortcomings with this simple parameterization. Errors in the correction model arising from an incomplete parameterization of solar radiation will, however, be minimized if the model is fitted using a similar range of environmental conditions to which it will be applied. In this case the errors in solar radiation will be similar in the model and data. However, it would be unrealistic to expect these errors to cancel if, for example, the training dataset contained only data from high latitudes and these coefficients were applied to data from the Tropics. If improved coefficients become available in the future, these can be used directly in the model. However, if it is thought desirable to use a different form of solar radiation parameterization, then the model will have to be rederived.

2) THERMAL RADIATIVE HEATING AND COOLING (Q_{LW})

The net rate of thermal radiative heating or cooling of the sensor environment will be the balance of the rate of heat lost to the atmosphere through radiative cooling and the rate of energy absorbed from the atmospheric downwelling longwave radiation; that is,

$$Q_{\text{LW}} = Q_{\text{LW\_ATMOS}} - Q_{\text{LW\_SHIP}}, \quad (6)$$

where Q_{LW} is the net rate of thermal heating or cooling for the sensor environment (W), $Q_{\text{LW\_ATMOS}}$ is the rate of atmospheric downwelling longwave radiation energy absorbed (W), and $Q_{\text{LW\_SHIP}}$ is the rate of heat loss due to radiative cooling (W).

The rate of cooling from the sensor environment can be estimated using the Stefan–Boltzmann law (e.g., Çengel 1998) and will be proportional to the surface

area of the sensor environment, A_{LW} (m^2), and the thermal emissivity ε_{LW}, that is,

$$Q_{LW\_SHIP} = A_{LW}\varepsilon_{LW}\sigma_{SB}T_{ship}^4, \quad (7)$$

where σ_{SB} is the Stefan–Boltzmann constant (5.67×10^{-8} W m^{-2} K^{-4}) and T_{ship} is the temperature of the sensor environment (K), T_{ship} can be expressed in terms of the air temperature and the heating error; that is,

$$T_{ship} = T_{air} + \Delta T_{err}, \quad (8)$$

where T_{air} is the air temperature (K) and ΔT_{err} the heating error (K). We can then write

$$T_{ship}^4 = T_{air}^4 + 4T_{air}^3\Delta T_{err} + 6T_{air}^2\Delta T_{err}^2 + 4T_{air}\Delta T_{err}^3 + \Delta T_{err}^4. \quad (9)$$

Assuming the air temperature is of the order 290 K and the heating errors are of the order 3 K, the last three terms are negligible compared to the first two. The rate of thermal cooling can then be approximated as

$$Q_{LW\_SHIP} = A_{LW}\varepsilon_{LW}\sigma_{SB}(T_{air}^4 + 4T_{air}^3\Delta T_{err}). \quad (10)$$

The downwelling longwave radiation must be estimated from the reported variables. Different longwave parameterizations are reviewed by Josey et al. (1997). Parameterizations are typically based on the air temperature, sea surface temperature (SST), total cloud cover, and vapor pressure. In this study we have used the model of Josey et al. (2003):

$$R_{LW} = \sigma_{SB}T_{eff}^4, \quad (11)$$

where R_{LW} is the atmospheric downwelling longwave radiation (W m^{-2}) and T_{eff} is the effective blackbody temperature of the atmosphere (K); T_{eff} is given by

$$T_{eff} = T_{air} + a_{lw}n^2 + b_{lw}n + c_{lw} + 0.84(D + 4.01) = T_{air} + \Delta T_{eff}, \quad (12)$$

where T_{air} is the air temperature (K), n is the fractional total cloud cover, and D is difference between the dewpoint temperature and the air temperature (K). The empirical coefficients are $a_{lw} = 10.77$, $b_{lw} = 2.34$, and $c_{lw} = -18.44$. Again the higher power terms of the temperature adjustment, ΔT_{eff}, are negligible when Eq. (12) is substituted into Eq. (11). Equation (11) then becomes

$$R_{LW} = \sigma_{SB}(T_{air}^4 + 4T_{air}^3\Delta T_{eff}). \quad (13)$$

Assuming that the thermal absorptivity of the ship is the same as the thermal emissivity (i.e., the ship acts as a blackbody) and the area normal to the downwelling longwave radiation is the same as the area emitting longwave radiation, the rate of longwave radiation absorbed is

$$Q_{LW\_ATMOS} = A_{LW}\varepsilon_{LW}\sigma_{SB}(T_{air}^4 + 4T_{air}^3\Delta T_{eff}). \quad (14)$$

Substituting Eqs. (10) and (14) into Eq. (6) gives a net thermal exchange of

$$Q_{LW} = A_{LW}\varepsilon_{LW}\sigma_{SB}(4T_{air}^3\Delta T_{eff} - 4T_{air}^3\Delta T_{err}). \quad (15)$$

It should be noted that due to the inclusion of the radiative heating and cooling of the sensor environment it will be possible to have a negative correction; that is, it would be possible to increase the MAT observations using such a correction. However, this will only occur during nighttime when there is no solar radiation to heat the sensor environment and when the convective and conductive heating is small. With increasing convective and conductive heating, the effect of longwave cooling will tend toward zero as the heat lost from the sensor environment will be regained from the atmosphere.

The formation of dew on the surfaces of the ship in contact with the atmosphere will also act to limit the longwave cooling of the ship's environment. If these surfaces are cooled by longwave radiation to below the dewpoint temperature, dew will form on them. The formation of dew releases latent heat and will warm the surfaces. The magnitude of this heating will depend on the rate of dew formation; however, we believe it will be of a similar magnitude to that from the longwave cooling. Maximum dewfall rates over grassland of 0.035 kg m^{-2} h^{-1} have been reported (Monteith 1957), and we here assume a maximum rate of dew formation of 0.1 kg m^{-2} h^{-1}, which indicates a maximum rate of latent heat release of 69 W m^{-2}. This is comparable to the net longwave (LW) heat flux between the atmosphere and the ships environment under clear skies. Where the rate of heating due to latent heat release is greater than the net longwave cooling, the object would warm above the dewpoint temperature and the formation of dew would stop. The conductive and convective cooling will also act to warm the object and will act to reduce dew formation.

Including the effect of latent heat release by dewfall in the model would add considerable complexity and would be expected to lead to limited improvements in a small fraction of the observations (for a combination of nighttime, clear skies, and low wind speeds). Any change in the temperature of the surfaces of the ship in contact with the atmosphere due to dewfall is likely to be a maximum of several tenths of a degree Celsius. The heating errors are proportional to the temperature difference between the ship environment and the atmosphere, hence any errors introduced into the heating error calculation by the exclusion of the effects of dewfall will be even smaller than this.

d. Convective and conductive cooling (Q_{CONV} + Q_{COND})

The modeling of both the convective and conductive cooling follow AB but are included here for completeness. The rate of convective and conductive heat loss from the sensor environment and instruments will be proportional to the temperature difference between the sensor environment and the air temperature. The rate of heat loss will also be proportional to the surface area

in contact with the atmosphere and to the convective and conductive heat transfer coefficients; that is,

$$(Q_{\mathrm{CONV}} + Q_{\mathrm{COND}}) = (T_{\mathrm{air}} - T_{\mathrm{ship}})A_c h_\mu + (T_{\mathrm{air}} - T_{\mathrm{ship}})A_c h_o, \quad (16)$$

where A_c is the surface area of the sensor environment in contact with the atmosphere (m^2), h_μ is the convective heat transfer coefficient (W m^{-2} K^{-1}), and h_o the conductive heat transfer coefficient (W m^{-2} K^{-1}), h_o is approximately constant over the range of MAT. However, h_μ depends on both the geometry of the ship and the relative wind speed and can be estimated from the empirically derived Nusselt number, Nu (e.g., Çengel 1998),

$$\mathrm{Nu} = \frac{h_\mu \delta}{k}, \quad (17)$$

where δ is a characteristic length (m) and k is the thermal conductivity of air (W m^{-1} K^{-1}). Approximating the geometry of the sensor environment as a block, the Nusselt number can be expressed in terms of the Reynolds (Re) and Prandtl (Pr) numbers as

$$\mathrm{Nu} = c_1\,\mathrm{Re}^{c_2}\,\mathrm{Pr}^{1/3}, \quad (18)$$

where c_1 and c_2 are constants dependant on the geometry of the sensor environment; Re can be written as a function of the relative wind speed, V (m s^{-1}), δ, and the kinematic viscosity of the air, ν (m^2 s^{-1}); that is,

$$\mathrm{Re} = \frac{V\delta}{\nu}. \quad (19)$$

Hence h_μ is given by

$$h_\mu = \frac{k\mathrm{Nu}}{\delta} = \frac{kc_1\left(\frac{V\delta}{\nu}\right)^{c_2}\mathrm{Pr}^{1/3}}{\delta}. \quad (20)$$

The Prandtl number (Pr) is a ratio of ν and the thermal diffusivity of air and is assumed constant over the range of temperatures encountered in the MAT; k can also be assumed constant over the range of temperatures encountered in the MAT measurements and δ will depend on the geometry and surface of the sensor environment and is constant for a fixed surface. These assumptions will allow us to group the different constants and unknowns together to give the convective heat transfer coefficient as a function of two coefficients to be derived empirically (x_3 and x_4, see Table 2) and the relative wind speed; that is,

$$h_\mu = x_3 V^{x4}. \quad (21)$$

e. Solution of the heat budget

Using the approximations and assumptions described in the previous sections, the heat budget [Eq. (1)] becomes

TABLE 2. Substitutions and empirical coefficients in the heat budget equations.

$x_1 = A_s\alpha_s/mc$	$h_1 = x_2(x_3V^{x4} + x_5)$
$x_2 = A_c/mc$	$h_2 = x_1R_{\mathrm{top}}(ak_1 + bk_1^2)$
$x_3 = \left[kc_1\left(\frac{\delta}{\nu}\right)^{c_2}\mathrm{Pr}^{1/3}\right]\Big/\delta$	$h_3 = x_1R_{\mathrm{top}}(ak_2 + 2bk_1k_2)$
$x_4 = c_2$	
$x_5 = h_o$	$h_4 = x_1R_{\mathrm{top}}bk_2^2$
$x_6 = A_{\mathrm{lw}}\varepsilon_{\mathrm{lw}}/mc$	$h_5 = x_64\sigma_{\mathrm{SB}}T_{\mathrm{ship}}^3\Delta T_{\mathrm{eff}}$
$k_1 = \sin(\mathrm{lat}\cdot dr)\sin(\mathrm{dec})$	$k_2 = \cos(\mathrm{lat}\cdot dr)\cos(\mathrm{dec})$

$$mc\frac{dT_{\mathrm{ship}}}{dt} = \alpha_s A_s R_s - (h_\mu + h_o)A_c\Delta T_{\mathrm{err}} + 4\varepsilon_{\mathrm{LW}}A_{\mathrm{LW}}\sigma_{\mathrm{SB}}T_{\mathrm{air}}^3(\Delta T_{\mathrm{eff}} - \Delta T_{\mathrm{err}}). \quad (22)$$

From Eq. (8) we can write

$$\frac{dT_{\mathrm{ship}}}{dt} = \frac{d(\Delta T_{\mathrm{err}} + T_{\mathrm{air}})}{dt} = \frac{d(\Delta T_{\mathrm{err}})}{dt} + \frac{d(T_{\mathrm{air}})}{dt}, \quad (23)$$

and assuming, as a first approximation, the diurnal cycle for the MAT is negligible, that is, $d(T_{\mathrm{air}})/dt = 0$, we then have

$$mc\frac{d(\Delta T_{\mathrm{err}})}{dt} + (h_\mu + h_o)A_c(\Delta T_{\mathrm{err}}) + 4\varepsilon_{\mathrm{LW}}A_{\mathrm{LW}}\sigma_{\mathrm{SB}}T_{\mathrm{air}}^3\Delta T_{\mathrm{err}} = \alpha_s A_s R_s + 4\varepsilon_{\mathrm{LW}}A_{\mathrm{LW}}\sigma_{\mathrm{SB}}T_{\mathrm{air}}^3\Delta T_{\mathrm{eff}}. \quad (24)$$

This approximation will not affect the solar radiative heating errors calculated using the solution of the heat budget [Eq. (27)]. However, if there is a diurnal cycle in the MAT, there may be other heating errors in the observations due to a lag between the atmospheric temperature and the temperature of the sensor environment. While it would be desirable to include this effect in the model, it has been excluded due to poor knowledge of the true diurnal cycle of MAT. It is expected that biases due to this effect would be an order of magnitude smaller than the radiative heating errors.

We can simplify Eq. (24) using order of magnitude considerations (see section a of appendix A). Term 3 on the lhs of Eq. (24) (the additional longwave cooling by the ship due to the temperature error) is shown to be negligible. The second term on the rhs of Eq. (24) expresses the imbalance between the longwave emissions by the ship and the atmosphere. The temperatures of the sensor environment and the atmosphere are similar (ΔT_{err} is of order a few kelvins), but the sensor environment is a more efficient emitter of longwave radiation than the atmosphere (the sensor environment is closer to being a blackbody than the atmosphere). The sensor environment therefore loses heat to the atmosphere by longwave emission and order of magnitude analysis shows that this term can be approximated as constant over the course of the day. Making these ap-

proximations for longwave radiation expanding the solar radiation term, and grouping together the unknown constants into coefficients to be determined empirically, x_1 to x_6 (see Table 2), we can write Eq. (24) as

$$\frac{d(\Delta T_{\text{err}})}{dt} + x_2(x_3 V^{x_4} + x_5)\Delta T_{\text{err}} = x_1[R_{\text{top}}(a_i + b_i \sin\theta)\sin\theta] + x_6 4\sigma_{\text{SB}} T_{\text{ship}}^3 \Delta T_{\text{eff}}. \quad (25)$$

Expanding the $\sin\theta$ terms and making further substitutions (see Table 2 and section b of appendix A), we can write Eq. (25) as

$$\frac{d(\Delta T_{\text{err}})}{dt} + h_1(\Delta T_{\text{err}}) = h_2 + h_5 + h_3 \cos(\alpha t + \beta) + h_4 \cos^2(\alpha t + \beta), \quad (26)$$

the solution of which is given by (full details are given in section c of appendix A)

$$(\Delta T_{\text{err}}) = \frac{h_2 + h_5}{h_1} + \frac{4\alpha^2 h_4}{4\alpha^2 + h_1^2}\left[\frac{\cos(\phi_t)\sin(\phi_t)}{2\alpha} + \frac{h_1 \cos^2(\phi_t)}{4\alpha^2} + \frac{1}{2h_1}\right] + \frac{\alpha h_3}{\alpha^2 + h_1^2}\left[\sin(\phi_t) + \frac{h_1}{\alpha}\cos(\phi_t)\right] + k_{\text{int}} \exp(-h_1\tau), \quad (27)$$

where k_{int} is the constant of integration and ϕ_t is the hour angle (see appendix A) at the time of observation, and τ is the time since sunrise. The constant of integration is found by solving Eq. (27) at sunrise, letting $\tau = 0$ and assuming the sensor environment is in equilibrium with the atmosphere at sunrise (appendix A). The nighttime heating error is calculated by allowing the heating error at sunset to decay exponentially up until the time of measurement, that is,

$$(\Delta T_{\text{err}}) = \frac{h_5}{h_1} + \Delta T_{\text{err,ss}} \exp(-h_1 \tau_{\text{ss}}), \quad (28)$$

where $\Delta T_{\text{err,ss}}$ is the heating error at sunset calculated using Eq. (27) and τ_{ss} is the time elapsed since sunset.

3. Application of the model

a. Introduction

In order to use the model derived above, the various empirical constants must be evaluated from a dataset containing estimates of the actual heating errors. Ideally comparisons of an air temperature sensor located, for example, on the bridge top could be compared with another, better exposed, sensor located far away from the ships influence. Measurements like this are, however, rare and do not exist at all for VOS. We therefore need to estimate the heating errors using the observations themselves and two methods for doing this will be described in section 3c. The observations that we have chosen to use were obtained on the OWS *Cumulus* during 1988 (section 3b). Due to the nonlinear solution to the heat budget we need to ensure that we are choosing the optimal solution, the method of doing this is described in section 3d.

b. Dataset

We use the observations made by the OWS *Cumulus* during 1988 for several reasons. The *Cumulus* made hourly observations at a single location giving information about the full diurnal cycle. During this period there were additional ''MultiMet'' research sensors onboard (Birch and Pascal 1987; Taylor et al. 1992). The MultiMet sensors included electrically aspirated psychrometers on the port and starboard sides of the OWS *Cumulus* adjacent to the Met Office screens, cup anemometers near each psychrometer to give the relative wind speed, and a weather vane near the port psychrometer to give the relative wind direction. Throughout 1988 the OWS *Cumulus* occupied Ocean Weather Station Lima (57.5°N, 20°W) in the North Atlantic, spending approximately 4 weeks on station at a time before returning to port. While on station the OWS *Cumulus* would normally drift beam to wind, only steaming to ensure the ship stays within a 30 n mi box about the nominal position (Taylor et al. 1992).

As an example of the data obtained, Fig. 1 shows the observations from the *Cumulus* made between 15 and 21 May 1988 (days 136–142). The dry-bulb air temperatures from the port and starboard psychrometers are shown in Fig. 1a along with the Met Office MAT and SST observations. SST varies little over the 6-day period ranging from 9.4°C during day 136 to 10.2°C during day 142. The diurnal cycle of the SST is small, varying by less than 0.5°C over the course of any day. In contrast, the nighttime MAT varies by several degrees Celsius over the period shown with a peak NMAT of 10.3°C during day 136 and a minimum value of 7.4°C during day 138. A strong diurnal cycle is present in the MAT observations from all three sensors, with the port psychrometer having the largest diurnal cycle. This is because the port psychrometer was on the leeward side of the ship for the majority of the observing period shown. From Figs. 1a and 1b it can be seen that the maximum differences between the MAT from the port and starboard psychrometers are found during days when the solar radiation is high and the relative wind speed is low, for example, days 136, 137, and 139 (Fig. 1b). The smallest difference between all three MAT sensors occurs during day 138, coinciding with the period of the lowest incident solar radiation and some of the higher wind speeds.

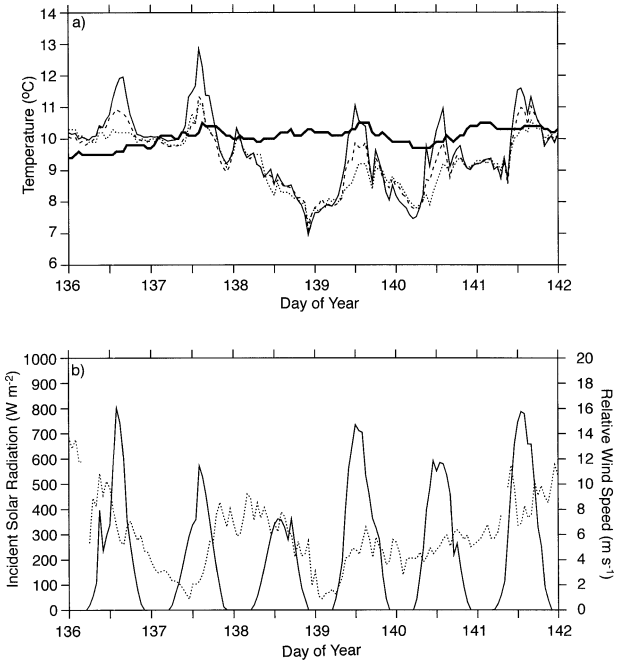

FIG. 1. An example of data from the OWS *Cumulus* [15 (day 136) to 21 (day 142) May 1988]. (a) Sea surface temperature (bold line) and marine air temperature (dotted line) from the Met Office sensors. Also shown are the port (solid line) and starboard (dashed line) air temperature measurements. (b) Incident solar radiation calculated using the okta model of Dobson and Smith (1988) (solid line) and relative wind speed (dotted line).

We have modeled the radiative heating errors in the leeward psychrometer (the port psychrometer for the observations shown in Fig. 1). The leeward sensor will be poorly exposed when the ship is drifting a beam the wind and therefore contains large errors. We exclude observations made when the wind is within 25° of the bow or stern since the exposure of the leeward sensor will vary under these conditions.

c. Estimation of the heating errors

The only information that we have about the heating errors is from the diurnal cycles of the observations themselves. We can make two different assumptions to get two different estimates of the errors. The first is that there is, on average, no diurnal cycle in air temperature and that all diurnal time-scale variations are due to radiative heating errors. This will overcorrect the observations by the magnitude of the real diurnal variations in air temperature, removing the diurnal cycle in the MAT from the observations. However, we expect the latter to be much smaller than the heating-induced temperature errors in the dataset. We estimate the heating errors by taking the difference from the nighttime mean MAT. If there is significant heat storage by the sensor environment we expect that heating errors will extend after sunset because of thermal lag. We therefore calculate the nighttime mean using only observations between local midnight and sunrise. This estimate of the heating errors will provide an upper limit to the estimated errors and the MAT correction fitted to these estimated errors.

An alternative estimate of the heating errors can be made by assuming that the diurnal variation of MAT − SST is negligible. In the same way as for MAT we can estimate the heating errors as the difference of the observations from the nighttime mean MAT − SST difference. The diurnal cycle in SST is likely to be larger than any real diurnal cycle in MAT. Thus, it is likely that using this method we will undercorrect the observations by removing the diurnal cycle in SST from the estimated errors. This method will provide a lower limit to the estimated errors and the MAT correction fitted to these estimated errors.

We can therefore make an estimate of the upper limit of the heating error by minimizing the diurnal cycle in MAT and an estimate of the lower limit by minimizing the diurnal cycle in the MAT − SST. If the heating errors are being estimated for a large group of ships such as the VOS a climatology of nighttime values can be calculated and the diurnal variation about this climatology used to derive the heating errors. Errors will be large for an individual observation, but should be random, so a large number of observations can be used to derive the model coefficients. Using a limited amount of data from a single ship means that we need to remove variability on time scales greater than a day to improve the estimates of the heating errors. For the OWS *Cumulus* MAT and SST observations the daily trends have been estimated by calculating a nighttime mean value from data between local midnight and sunrise for each day and then linearly interpolating between these nighttime means. The trend is then subtracted from the MAT or the MAT − SST differences to give the estimate of the heating error. Using this method we have had to discard any observations where the MAT changes rapidly, such as during the passage of a cold front, since a rapid change in the MAT can lead to poor estimates of the daily trend in both the MAT and the MAT − SST difference and also of the heating errors themselves. In this paper we have excluded any observations where the daily trend in the MAT exceeds ±1.5°C from the fitting routine, however, we will still correct these observations.

Figure 2a shows the MAT − SST differences for the dataset example shown in Fig. 1. Also shown in Fig. 2a is the trend in the MAT − SST differences, calculated using the method described above, with the cold front during day 138 clearly visible. There is a strong diurnal cycle in the MAT − SST differences, suggesting a strong diurnal cycle in the estimated heating errors. Figure 2b shows the estimated heating errors calculated using the MAT − SST differences (solid line) and using only the MAT (dashed line). The estimated errors calculated using both methods are very similar with differences of less than 0.1°C on average. The effect of

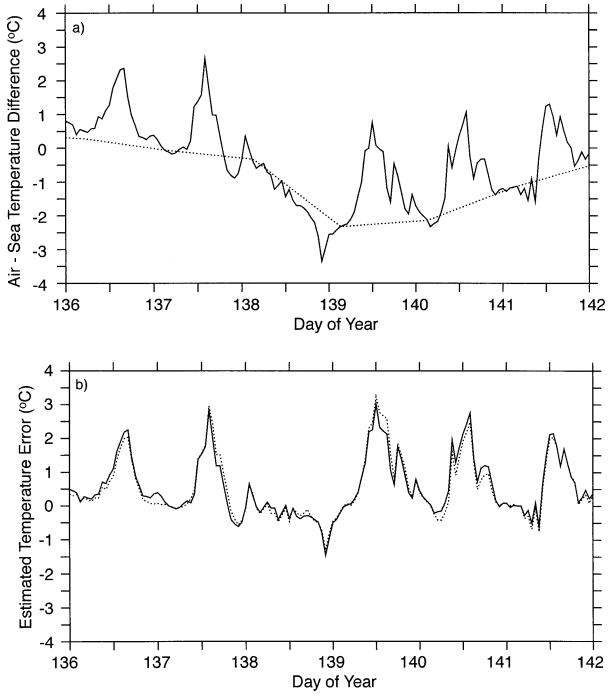

FIG. 2. (a) Air − sea temperature difference (solid line) and estimated trend in air − sea temperature difference (dotted line) between 15 and 21 May 1988. (b) Estimated errors between 15 and 21 May calculated using the air − sea temperature difference (solid line) and the MAT (dotted line).

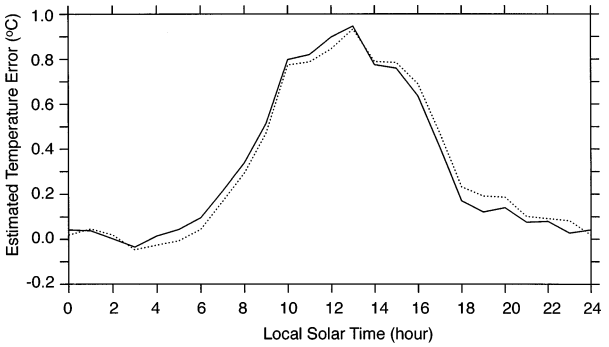

FIG. 3. Diurnal cycle showing the hourly average estimated errors for 1988 calculated using the air − sea temperature differences (solid line) and the MAT (dotted line).

the cold front on the estimated errors can also be seen in Fig. 2b, with negative heating errors throughout most of day 138.

Figure 3 shows the estimated errors for the whole 1988 dataset calculated using the two methods and averaged against the local solar time. As expected in this northerly region with strong wind speeds the difference between the two error estimates are small, implying that the diurnal cycles in both MAT and SST are small. In some other regions these diurnal effects will be much more important. The estimated heating errors are slightly larger in the afternoon compared to a similar time in the morning. There may be some indication that there is a phase difference between the error estimates consistent with the SST diurnal cycle leading the MAT; differences are, however, small.

d. Fitting the model coefficients

We fit the solution of the heat budget [Eq. (27)] to the estimated errors by minimizing the sum of the squared differences between the solution of the heat budget and the estimated errors. The fitting routine used is the nonlinear least squares regression subroutine E04UNF from the Numerical Algorithms Group library (NAG 2002). To ensure that the fitted solution is independent of the data to which it is being applied we have divided the dataset into two randomly chosen subsets, one subset of 500 observations to use as the training set and one subset of 800 of the remaining 1245 observations to use as the evaluation set. Figures 4a and 4b show the estimated errors (calculated using the MAT − SST differences) for the two subsets of data averaged over a 24-h cycle. The two subsets are similar, as would be expected, with peak estimated errors of around 1.0°C between 1200 and 1300 h local solar time. The average estimated error of training subset is 0.33°C with a root-mean-square error of 0.79°C. For the evaluation subset the average estimated error and rmse are 0.31° and 0.74°C, respectively.

As the solution of the heat budget equation is nonlinear (with respect to the fitted coefficients) it is possible to obtain different solutions depending on the starting values chosen for the empirically fitted coefficients (x_1 to x_6, see Table 2) and their allowed ranges. Some of these solutions will be related, for example, the coefficients may be scaled; however, local minima may also exist. For very poorly chosen initial values and ranges it is actually possible to obtain a solution that increases the sum of squared differences. To ensure the fitted values are not a local minima and that we have the best fit possible we have run the fitting routine 500 times for a subset of the observations. Each run has different initial values for the coefficients that are randomly generated within the chosen bounds. To avoid different solutions, that are similar, but scaled, we have set the value of x_1 at 0.01. The limits for the other coefficients are given in Table 3.

Table 4 shows a summary of the fitted coefficients for the top 100 runs using the estimated errors based on the MAT − SST differences, ranked on the reduction in rmse. Table 4 shows that, even though we have fixed the value of the x_1, there is still a considerable variation in the other coefficients. For example, the average fitted value of x_3 is 28.7 with a standard deviation of 8.8 (30.8% of the average value). Variation of the other fitted coefficients ranged from 17.4% for x_4 to 45.1% for x_6. While this variation in individual coefficients is

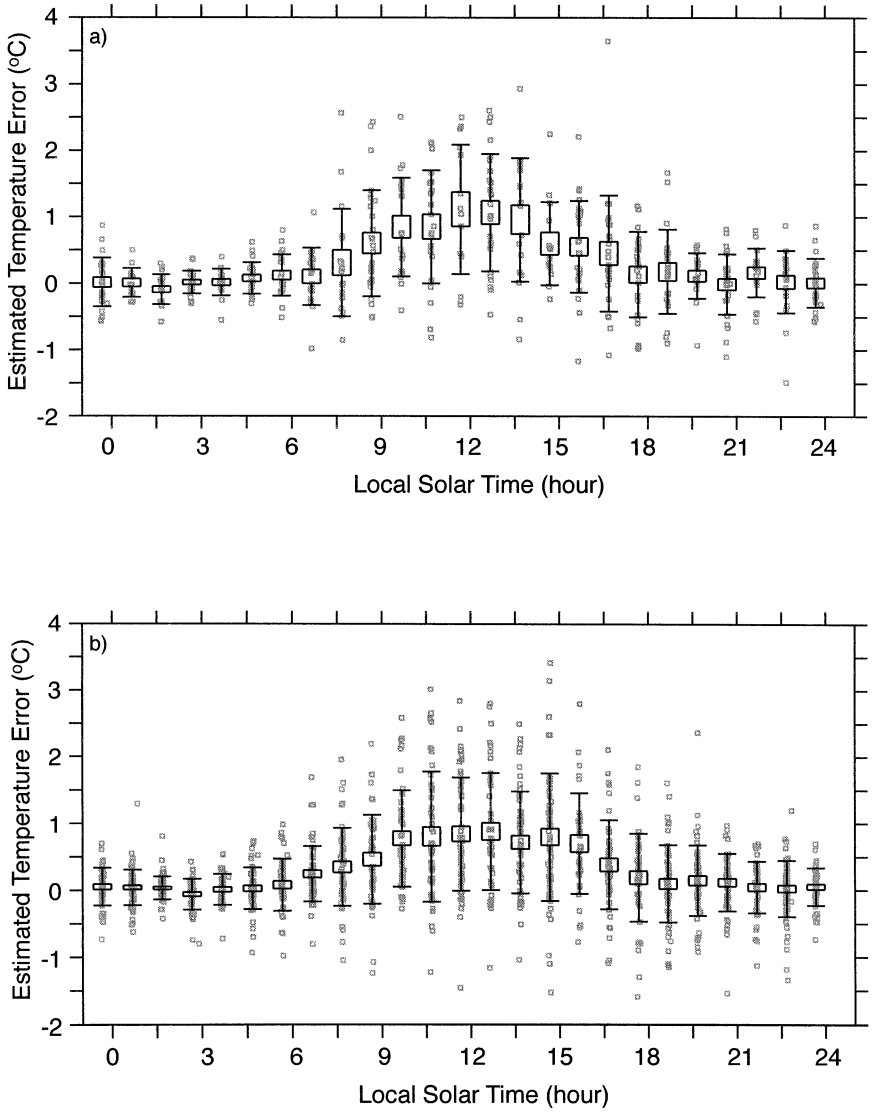

FIG. 4. (a) Estimated errors calculated using the MAT − SST differences plotted against local solar time for the training subset. The center of the boxes indicate the average hourly value, the outside of the boxes the standard error, and the error bars the standard deviation. The gray squares are the individual observations. (b) As in (a) but for the evaluation subset.

large, the variation in the value of the solution and in the reduction of the rmse is relatively small. The average reduction in the rmse is 33.6% with a standard deviation of 0.10% (0.1% of the average value).

TABLE 3. Lower and upper limits for initial x values in fitting routine.

	Lower limit	Upper limit
x_1	0.01	0.01
x_2	0.01	0.10
x_3	20	100
x_4	0.2	2.0
x_5	40	400
x_6	0	0.02

The range of values of the solution given by the 100 runs with the greatest reduction in rmse is shown in Fig. 5a. The solution of the heat budget was calculated every hour using the coefficients from each of the 100 runs and fixed, typical environmental parameters of relative wind speed: 8 m s^{-1}, total cloud cover: 4 oktas, marine air temperature: 12°C, dewpoint: 9°C, day: 200 (19 July), and latitude: 57.5°N. The average hourly value has been plotted against local solar time with the error bars indicating the standard deviation of the average hourly values. Figure 5a shows that the actual values of the solution varied little over these 100 runs, with a peak value of 2.04 ± 0.02°C. This small variation in the value of the solution and in the reduction in the rmse compared to the large variation in the individual coef-

TABLE 4. Summary of fitted values for top 100 runs using the estimated errors from the air − sea temperature difference and the training set.

	Best	Median	Mean	Std dev (% of mean value)
x_1	0.01	0.01	0.01	0.0 (0%) (fixed)
x_2	0.0100	0.0172	0.0170	0.00473 (27.8%)
x_3	20.0	27.0	28.7	8.8 (30.8%)
x_4	0.771	0.485	0.500	0.087 (17.4%)
x_5	284.0	146.0	162.0	54.4 (33.6%)
x_6	0.000 350	0.000 485	0.000 465	0.000 210 (45.1%)
$x_2x_3V^{x4}$	0.99	1.29	1.29	0.17 (13.2%)
x_2x_5	2.84	2.51	2.51	0.16 (6.4%)
$x_2(x_3V^{x4} + x_5)$	3.83	3.81	3.80	0.03 (0.9%)
Residual error	0.0186	0.0170	0.0172	0.0027 (15.6%)
Percent reduction in rmse	33.6	33.5	33.5	0.05 (0.2%)

ficients is due to the inverse correlation between the convective and conductive cooling terms ($x_2x_3V^{x4}$ and x_2x_5) and the small influence x_6 has on the daytime values. Over the top 100 runs the correlation coefficient between $x_2x_3V^{x4}$ and x_2x_5 is -0.98 for a wind speed of 8 m s^{-1}; that is, an increase in the convective cooling term ($x_2x_3V^{x4}$) will be almost matched by a decrease in the conductive cooling term (x_2x_5). The average value of the combined convective and conductive cooling terms [$x_2x_3V^{x4} + x_2x_5$; i.e., h_t in Eq. (A6)] is 3.80 with a standard deviation of 0.03.

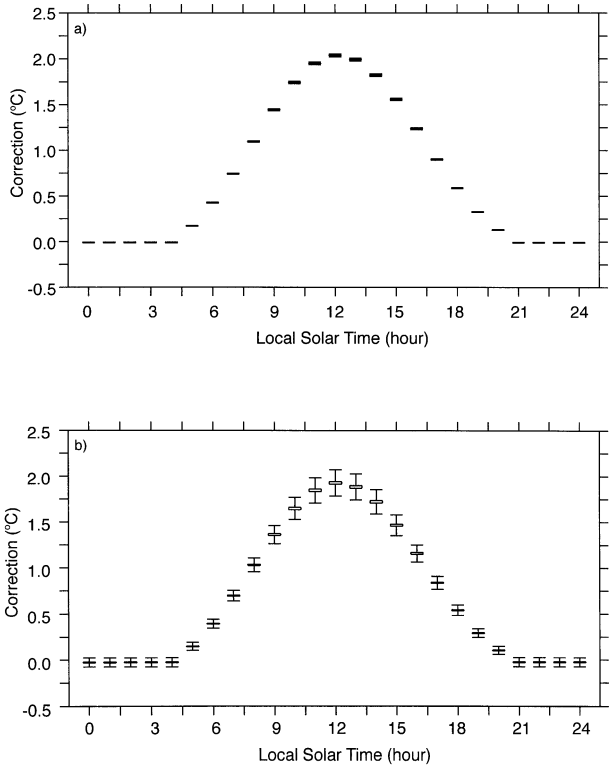

FIG. 5. (a) Range of values for the solution of the heat budget calculated using the fitted coefficients (fitted to the training subset) from the 100 runs with the greatest reduction in rmse. The values of the solution have been calculated using fixed environmental conditions of relative wind speed: 8 m s^{-1}, total cloud cover: 4 oktas, marine air temperature: 12°C, dewpoint: 9°C, day: 200 (19 Jul), and latitude: 57.5°N. The boxes indicate the mean value (center) and standard error (outside). The error bars indicate the standard deviation. (b) As in (a) but for the top 100 runs fitted to random subsets.

Table 5 shows a summary of the statistics for the top 100 runs of the fitting routine for the estimated errors based only on the MAT. The variation of the fitted coefficients is similar to that found in using estimates of the heating errors based on the MAT − SST differences and that this variation does not result in a large variation in the percentage reduction of the rmse or of the residual errors. Again this is due to the anticorrelation between the convective and conductive cooling terms (correlation coefficient = -0.98 for a wind speed of 8 m s^{-1}). A similar value for the sum of the convective and conductive cooling was found using the MAT-based error estimates as was found using the MAT − SST difference-based estimates. The average value of the convective and conductive cooling using the MAT-based estimates was 3.90 with a standard deviation of 0.04, compared to a average value of 3.80 ± 0.03 for the errors estimates based on the MAT − SST differences.

e. Estimated accuracy of fit

To gain an indication of the accuracy of the fit and the impact that the selection of the subset used in the fit has on the fitted coefficients we have run the fitting routine an additional 500 times. In each run the subset used is selected randomly from the whole dataset and the initial values of the coefficients are generated as described above. Table 6 shows the summary statistics for the top 100 runs using the estimated errors selected from the whole dataset. While the variation in the coefficients x_2–x_5 has increased, with a maximum variation of 62.1% for x_5, the variation in the convective and conductive cooling is still small, with an average value of 4.01 and a standard deviation of 0.33 (cf. to 3.80 ± 0.03 for the fitting routine using a single subset). Figure 5b is similar to Fig. 5a but calculated using the coefficients from the 100 runs with the greatest reduction in rmse fitted to random subsets of 500 observations

TABLE 5. As in Table 4 but for the error estimates based on the MAT.

	Best	Median	Mean	Std dev (% of mean value)
x_1	0.01	0.01	0.01	0.0 (0%) (fixed)
x_2	0.0100	0.0142	0.0154	0.0044 (28.7%)
x_3	20.0	22.7	26.0	7.1 (27.5%)
x_4	0.882	0.656	0.677	0.115 (17.1%)
x_5	263	155	168	55 (32.6%)
x_6	0.0	0.0	0.0	0.000 (0%)
$x_2x_3V^{x4}$	1.25	1.54	1.53	0.18 (11.6%)
x_2x_5	2.63	2.36	2.37	0.17 (7.3%)
$x_2(x_3V^{x4} + x_5)$	3.88	3.89	3.90	0.04 (0.9%)
Residual error	0.0169	0.0161	0.0169	0.0026 (15.5%)
Percent reduction in rmse	34.8	34.7	34.7	0.04 (0.1%)

from the whole dataset. The MAT − SST estimate of the heating errors has been used. The peak value of the solution is 1.93 ± 0.14°C compared to 2.04 ± 0.02°C for the training subset (Fig. 5a). Figures 5a and 5b show that fitting the solution of the heat budget to randomly selected subsets results in a larger variation in the value of the solution and fitted coefficients compared to fitting the coefficients to a single subset. This is to be expected due to the larger scatter in the randomly selected subsets (e.g., Figs. 4a and 4b). The results suggest the accuracy of the solution should be of the order of ±0.2°C.

4. Results and discussion

Figure 6a shows the estimated errors from the evaluation subset (i.e., the subset of data independent of the fitting routine) calculated using the MAT − SST difference averaged against local solar time. Also shown are the solutions of the heat budget and the residual estimated errors after the MAT have been corrected using the solution of the heat budget. The solution of the heat budget reproduces the average diurnal cycle seen in the heating errors fairly accurately. After correction the heating errors have been largely removed from the observations; the average estimated error in the evaluation subset has been reduced from 0.31° to 0.03°C. The rmse has similarly been reduced from 0.74°C before correction to 0.52°C, a change of approximately 30%. While the maximum hourly average residual errors may be as large as 0.2°C, this lies within the expected accuracy of the fitting routine and solution of the heat budget (section 3e). The maximum hourly residual errors also lie just within the upper limit of the required accuracy of 0.2°C for flux calculation to within 10 W m^{-2} (Taylor et al. 2000), typical errors are much smaller. The correlation coefficient between the estimated errors and the solution of the heat budget is 0.64.

Figure 6b shows the same information for the heating errors calculated using the MAT observations. As would be expected, given the similarity between the estimated errors from the two methods, the results are similar to those shown in Fig. 6a. After correction we have removed the diurnal cycle of the estimated heating errors and the average estimated error has been reduced from 0.31°C before correction to 0.03°C after correction. The rmse has been reduced from 0.75° to 0.55°C (a change of approximately 27%) and the correlation coefficient between the estimated errors and the solution of the heat budget is 0.54.

The estimated heating errors calculated using the MAT − SST differences are shown in Fig. 7a for the period 15–21 May 1988. Also shown are the correction (dashed line) and residual heating errors (solid line). While the correction is only expected to be accurate when averaged over a large amount of data, Fig. 7a suggests that the model reproduces and removes the individual diurnal cycles relatively accurately. Figure 7b shows the corrected MAT observations (solid line)

TABLE 6. As in Table 4 but for the whole dataset.

	Best	Median	Mean	Std dev (% of mean value)
x_1	0.01	0.01	0.01	0.0 (0%) (fixed)
x_2	0.0143	0.0161	0.0170	0.0064 (37.4%)
x_3	100.0	36.7	47.9	26.8 (56.0%)
x_4	0.433	0.586	0.608	0.231 (37.9%)
x_5	49.0	80.1	100.2	62.2 (62.1%)
x_6	0.000	0.000	0.00129	0.00244 (189%)
$x_2x_3V^{x4}$	3.52	2.47	2.50	0.78 (31.3%)
x_2x_5	0.702	1.584	1.514	0.627 (41.4%)
$x_2(x_3V^{x4} + x_5)$	4.22	4.01	4.01	0.34 (8.4%)
Residual error	0.0298	0.0374	0.0447	0.0300 (67.1%)
Percent reduction in rmse	37.6	34.5	34.7	1.2 (3.6%)

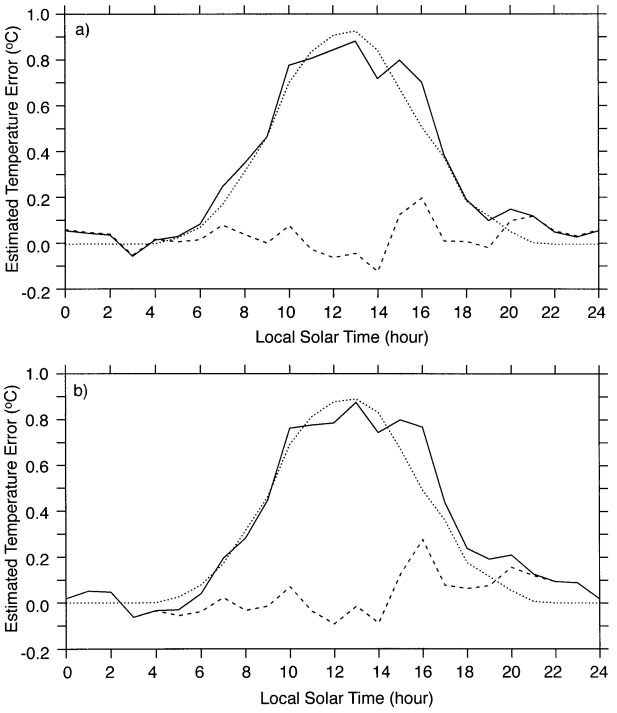

FIG. 6. (a) Diurnal cycle of the hourly average estimated error (solid line), correction (dotted line), and residual estimated error (dashed line) for the estimated errors calculated using the air − sea temperature differences from the evaluation subset. (b) As in (a) but for the MAT estimate of the heating errors.

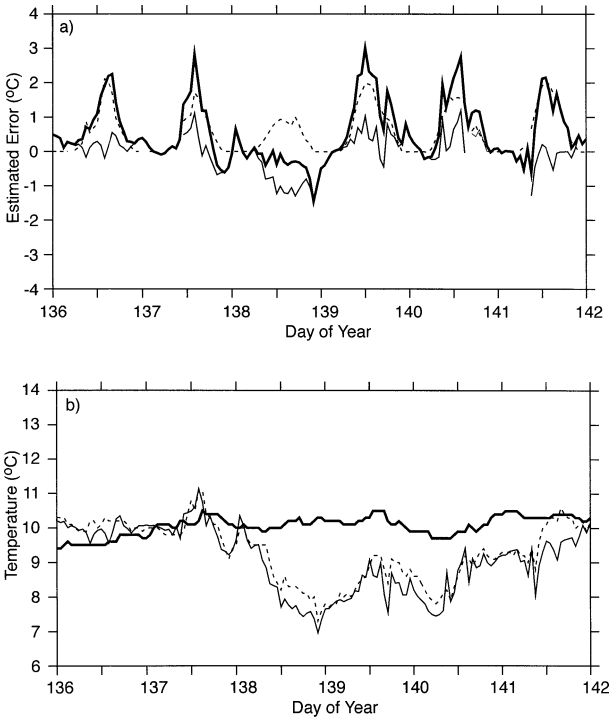

FIG. 7. (a) Example of the estimated errors (bold line), correction (dashed line), and residual estimated error (solid line) calculated using the air − sea temperature differences, shown for the period 15–21 May 1988. (b) The sea surface temperature (bold line) and marine air temperature (dashed line) from the Met Office sensors for the period 15–21 May. Also shown is the corrected port psychrometer air temperature (solid line; cf. Fig. 1a).

from the leeward psychrometer (in this case the port psychrometer) for the same period. Also shown are MAT from the Met Office sensor (dashed line) and SST (bold line). When Figs. 1a and 7b are compared we see that the MAT − SST differences calculated using the leeward psychrometer are much more realistic. The diurnal cycle of MAT has been greatly reduced for individual days. From Fig. 7b it can also be seen that the corrected MAT observations from the leeward psychrometer are colder than the MAT observations from the Met Office screen. This suggests that the windward Met Office screen experiences a smaller, but observable, solar heating effect. This suggests that, if we had used the difference between the psychrometers and the Met Office screens as an estimate of the heating errors, we would have underestimated the true errors.

It should be noted that the heat storage seen in the *Cumulus* observations (i.e., the persistence of the errors in the afternoon) is relatively small due to the small size of the ship, the northerly location of Ocean Weather Station Lima (57.5°N), and the practice of the *Cumulus* to drift beam on to the wind. However, even with this small heat storage taken into account an asymmetry about midday can be seen, heating errors in the afternoon are up to 0.2°C warmer than at a similar time in the morning. Figure 8a shows that heating errors calculated using the solution of the heat budget plotted against the time of day for the typical environmental parameters used previously. Also shown are the same heating errors mirrored about midday, with the morning values projected onto the afternoon. The difference between the two curves is shown in Fig. 8b; it ranges up to 0.2°C in the afternoon. Heat storage will be even more important for large ships, such as VOSs, operating in lower latitudes.

5. Summary and conclusions

In this paper the development of a new correction to remove the solar heating bias in ship MAT observations has been presented. The first challenge is to estimate the size of the bias. Two different methods have been used to estimate the size of the heating errors in the example dataset of OWS *Cumulus* data. One method minimizes the diurnal variation in air temperature and will lead to an overestimate of the heating error; the other minimizes the diurnal variation in air − sea temperature difference and should underestimate the heating error. For the OWS *Cumulus* data the two estimates are very similar as the diurnal cycles in both air and sea temperature are small in this high-latitude region. For other datasets either in lower latitudes or global datasets,

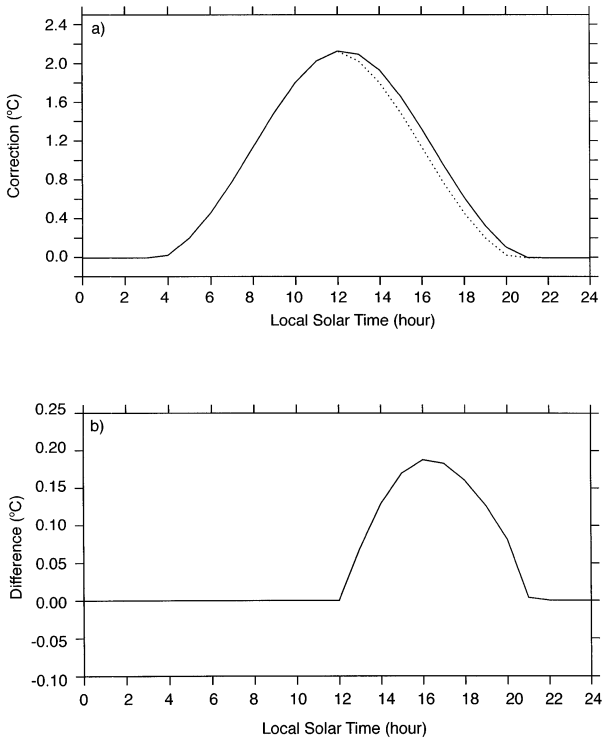

FIG. 8. (a) Solution of the heat budget (solid line) calculated using set environmental parameters of relative wind speed: 8 m s^{-1}, total cloud cover: 4 oktas, marine air temperature: 12°C, dewpoint: 9°C, day: 200 (19 Jul), and latitude: 57.5°N. Also shown is the solution of the heat budget from the morning mirrored about 1200 h local solar time (dotted line). (b) The difference between the two lines in (a).

such as ICOADS, the difference between the two estimates should be larger and will give an upper and lower error bound on the estimate of the heating error. The two methods for deriving error estimates presented in this paper should ideally be used together to provide upper and lower bounds on the estimated errors.

The correction developed has been designed to minimize the estimated air temperature errors due to the solar radiative heating of the sensor environment by modeling the heat exchange between the ship and the atmosphere, allowing for heat storage by the ship and time-varying solar heating. This is the first time that heat storage by the ship has been included in a correction for the solar heating. This model will therefore be able to recover the true diurnal cycle of air temperature in cases where there is significant heat storage. The thermal characteristics of the ship are estimated by fitting six different coefficients that combine characteristics such as the solar absorptivity, conductive heat transfer coefficient, and surface area of the region of the ship near to the air temperature sensor. The heating error varies with the incoming solar radiation (which is estimated from the cloud cover) and the *relative wind speed* over the ship and these environmental variables are required to calculate the correction. The coefficients are adjusted to minimize the estimated correction for a random subset of the dataset for which a correction is required, in our case that for the OWS *Cumulus* in 1988.

When the correction is applied to an independent subset of OWS *Cumulus* data the average estimated heating error, based on estimates of the heating error from MAT − SST, is reduced from 0.31° to 0.03°C. The root-mean-square error is similarly reduced from 0.74° to 0.52°C, a reduction of about 30%. When the correction is fitted to estimates of the heating errors based only on the MAT observations similar results are found, with the average heating error again reduced from 0.31° to 0.03°C. The reduction in the rmse is slightly less, with a reduction from 0.75° to 0.55°C. The results of fitting the correction using a Monte Carlo approach suggests the correction should have an accuracy of about ±0.2°C. In addition to significantly reducing the average heating error and rmse, the correction removes the average diurnal cycle of the heating errors. The hourly average residual errors lie within the expected accuracy of the correction (e.g., Fig. 6) and also within the upper limit of ±0.2°C for flux calculation to within 10 W m^{-2}. The individual diurnal cycles in the OWS *Cumulus* data are also improved by the correction (Fig. 7).

It should be emphasized that the coefficients presented in this paper are only valid for the OWS *Cumulus.* Additionally, the training dataset used to determine the coefficients needs to be selected carefully to ensure that it is fully representative of observations to which the correction will be applied. This will minimize any correlated errors between the parameterizations used and the model.

Although the coefficients presented will only be valid for the OWS *Cumulus,* the model can be fitted to estimate air temperature errors for any ship. It is expected to perform equally well for observations from different classes of ships, such as the VOS. If fitted to data from classes of ships, we would not expect the correction to be accurate for individual observations, but rather to the means of a large number of observations from many ships over a period of a month or longer. When applied in this way the correction will improve the quality of daytime air temperature observations in ICOADS. In D. I. Berry et al. (2004, unpublished manuscript) we will fit and apply the model to different classes of ships from the ICOADS to estimate and correct the radiative heating errors in MAT observations from VOS.

Acknowledgments. This work was supported by funding from the U.K. Government Meteorological Research Programme. The authors thank the reviewers for comments that have strengthened the paper. The authors wish to acknowledge use of the Ferret program for analysis and graphics in this paper. Ferret is a product of NOAA's Pacific Marine Environmental Laboratory. (Information is available online at www.ferret.noaa.gov.)

APPENDIX A

Simplification and Solution of the Heat Budget

a. Longwave approximations

From section 2e, we have Eq. (24):

$$mc\frac{d(\Delta T_{\text{err}})}{dt} + (h_\mu + h_o)A_c(\Delta T_{\text{err}}) + 4\varepsilon_{\text{LW}}A_{\text{LW}}\sigma_{\text{SB}}T_{\text{air}}^3\Delta T_{\text{err}} = \alpha_s A_s R_s + 4\varepsilon_{\text{LW}}A_{\text{LW}}\sigma_{\text{SB}}T_{\text{air}}^3\Delta T_{\text{eff}}.$$

By comparing the magnitudes of the different components we can show that the longwave cooling on the lhs of Eq. (24) can be assumed negligible under most conditions and that the longwave cooling on the rhs can be assumed constant.

From Eq. (20) we have

$$h_\mu = \frac{kc_1\left(\frac{V\delta}{\nu}\right)^{c_2}\text{Pr}^{1/3}}{\delta}.$$

Letting $T_{\text{air}} = 303$ K we then have $\nu = 16.01 \times 10^{-6}$ m^2 s^{-1}, $k = 26.38 \times 10^{-3}$ W m^{-1} K^{-1}, and Pr = 0.712 (Chapman 1984). The constants c_1 and c_2 will depend on the geometry of the ship and for noncircular cylinders range from 0.0385 to 0.246 and 0.588 to 0.782, respectively (Chapman 1984). For flow over a flat plane $c_1 = 0.332$ and $c_2 = 0.5$ (Chapman 1984). To gain an idea of the magnitude of h_μ we have used values of 0.15 and 0.6 for c_1 and c_2, respectively. Assuming that the surfaces on the ship have a characteristic length of the order of 1 cm (0.01 m) and that the relative wind speed is 8 m s^{-1}, we can then write h_μ as

$$h_\mu = \frac{0.026\,38 \times 0.15\left(\frac{8 \times 0.01}{16.01 \times 10^{-6}}\right)^{0.6}0.712^{1/3}}{0.01} = 58.5 \text{ W m}^{-2}\text{ K}^{-1}. \quad \text{(A1)}$$

Assuming the value of the conductive heat transfer coefficient is approximately 20 W m^{-2} K^{-1}, the total convective and conductive heat transfer coefficient is approximately 78.5 W m^{-2} K^{-1}. Hence we can write the convective and conductive cooling as

$$(h_\mu + h_o)A_C\Delta T_{\text{err}} = 78.5A_C\Delta T_{\text{err}}. \quad \text{(A2)}$$

We can similarly estimate the magnitude of the longwave cooling on the lhs. Letting the thermal emissivity be equal to 0.9 and the air temperature 303 K, we can write the cooling term on the lhs as

$$4\varepsilon_{\text{LW}}A_{\text{LW}}\sigma_{\text{SB}}T_{\text{air}}^3\Delta T_{\text{err}} = 4 \times 0.9 \times A_{\text{LW}} \times 5.67 \times 10^{-8} \times 303^3 \times \Delta T_{\text{err}} = 5.68A_{\text{LW}}\Delta T_{\text{err}}. \quad \text{(A3)}$$

If the areas cooled by the longwave cooling (A_{LW}) and the convective and conductive cooling (A_{C}) are the same then from Eqs. (A2) and (A3), we can see that the longwave cooling is less than 8% of the convective and conductive cooling. However, some of the longwave radiation emitted is likely to be reabsorbed by the sensor environment, so this value represents an upper limit for the effect of the longwave cooling. As the longwave cooling on the lhs of Eq. (24) is small compared to the convective and conductive cooling we can drop the longwave term with the introduction of only a small error.

Due to the assumption that the diurnal cycle of the MAT is negligible and that the environmental conditions do not change over the course of the day we can approximate the longwave term on the rhs of Eq. (24) as constant. Even though we do not know the true air temperature, we can use the observed air temperature to calculate the longwave term with the introduction of a small error into the solution of the heat budget and the estimated errors (<3% of the estimated error). We can examine the size of this error by looking at the solution of the heat budget [Eq. (27)] and the term that includes the longwave cooling (i.e., h_5/h_1):

$$(\Delta T_{\text{err}}) = \frac{h_2 + h_5}{h_1} + \frac{4\alpha^2 h_4}{4\alpha^2 + h_1^2}\left[\frac{\cos(\phi_t)\sin(\phi_t)}{2\alpha} + \frac{h_1\cos^2(\phi_t)}{4\alpha^2} + \frac{1}{2h_1}\right] + \frac{\alpha h_3}{\alpha^2 + h_1^2}\left[\sin(\phi_t) + \frac{h_1}{\alpha}\cos(\phi_t)\right] + k_{\text{int}}\exp(-h_1 t)$$

$$h_5 = 4x_6\sigma_{\text{SB}}T_{\text{air}}^3[10.77n^2 + 2.34n - 18.77 + 0.84(T_{\text{dew}} - T_{\text{air}} + 4.01)]$$

$$h_1 = x_2(h_\mu + h_o)$$

$$x_2 = \frac{A_c}{mc}, \qquad x_6 = \frac{\varepsilon_{\text{LW}}A_{\text{LW}}}{mc}.$$

Letting the measured air temperature be 303 K, the dewpoint temperature 299.2 K (a dewpoint depression of −3.8°C and a relative humidity of approximately 80%), and the cloud cover 5 oktas ($n = 5/8$), h_5 becomes

$$h_5 = 4x_6 5.67 \times 10^{-8} \times 303^3[10.77 \times 0.625^2 + 2.34 \times 0.625 - 18.77 + 0.84(-3.8 + 4.01)] = -81.54x_6.$$

Using the values of h_μ and h_o given above h_1 becomes $78.5x_2$. Assuming a thermal absorptivity of 0.9 and that A_C and A_{LW} are equal, h_5/h_1 becomes -0.93°C. If there is a 3°C error in the air temperature measurement (i.e., the true value for T_{air} should be 300 K), then the correct value of h_5/h_1 would be equal to -0.91°C. Hence by using the measured value of T_{air} we are overestimating the h_5/h_1 term by -0.03°C, an error of approximately 3%. As the heating error decreases, so does the error in h_5/h_1, with an error of 1% for a heating error of 1°C. This error value (as a percentage of h_5/h_1) is independent of the convective and conductive cooling and also of the areas exposed to the longwave cooling and the convective and conductive cooling. Since the heating errors are rarely larger than 3°C this suggest the maximum error introduced through using the observed air temperature should be no larger than 3%.

b. Simplification of the heat budget equation

Before we can solve the heat budget, Eq. (25), we need to expand the $\sin\theta$ terms as a function of time.

$$\frac{d(\Delta T_{err})}{dt} + x_2(x_3V^{x_4} + x_5)\Delta T_{err} = x_1[R_{top}(a_i + b_i \sin\theta)\sin\theta] + x_6 4\sigma_{SB}T_{ship}^3\Delta T_{eff}.$$

The solar elevation, $\sin\theta$, is given by

$$\sin\theta = \sin(\text{lat}\cdot dr)\sin(\text{dec}) + \cos(\text{lat}\cdot dr)\cos(\text{dec})\cos(\phi), \quad \text{(A4)}$$

where lat is the latitude (deg), dr is $\pi/180$, dec is the declination of the sun (rad), and ϕ is the hour angle (rad). The hour angle and declination have been calculated using

$$\text{dec} = -23.5\sin[(80 - \text{day})dr]dr \quad \text{(A5)}$$

$$\phi = \left[(12 - \text{utc})\frac{360}{24} - \text{lon}\right]dr, \quad \text{(A6)}$$

where lon is the longitude (deg), utc is the time (UTC), and day is the day of year. Substituting Eq. (A4) into Eq. (25) gives

$$\frac{d(\Delta T_{err})}{dt} + x_2(x_3V^{x_4} + x_5)\Delta T_{err} = x_1R_{top}[(ak_1 + bk_1^2) + (ak_2 + 2bk_1k_2)\cos(\alpha t + \beta) + bk_2^2\cos^2(\alpha t + \beta)] + x_6 4\sigma_{SB}T_{ship}^3\Delta T_{eff}, \quad \text{(A7)}$$

where $k_1 = \sin(\text{lat}\cdot dr)\sin(\text{dec})$, $k_2 = \cos(\text{lat}\cdot dr)\cos(\text{dec})$, and $\alpha t + \beta = [(12 - \text{utc})\,360/24 - \text{lon}]\,dr$ = hour angle (ϕ); β and t will depend on the longitude and reference period, respectively, and $\alpha = -\pi/12$. Equation (A7) can be further simplified to give

$$\frac{d(\Delta T_{err})}{dt} + h_1(\Delta T_{err}) = h_2 + h_5 + h_3\cos(\alpha t + \beta) + h_4\cos^2(\alpha t + \beta), \quad \text{(A8)}$$

where h_1–h_5 are given in Table 2.

c. Solution of the heat budget

From section 2 we have a simplified model of the heat budget for an idealized ship [Eq. (26)], balancing the heating and cooling terms with the energy stored:

$$\frac{d(\Delta T_{err})}{dt} + h_1(\Delta T_{err}) = h_2 + h_5 + h_3\cos(\alpha t + \beta) + h_4\cos^2(\alpha t + \beta),$$

where ΔT_{err} is the heating error (°C), t is the time (s), h_1–h_5 coefficients constant with time (see Table 2 for definitions); and α and β are constants used in the conversion of time (UTC) and longitude to hour angle ($\alpha t + \beta$) (see appendix Ab). Equation (26) can be solved by letting

$$P(t) = h_1$$

$$Q(t) = h_2 + h_5 + h_3\cos(\alpha t + \beta) + h_4\cos^2(\alpha t + \beta),$$

and using the integrating factor

$$\mu(t) = \exp\left[\int P(t)\,dt\right] = \exp(h_1 t).$$

The solution of Eq. (26) is then given by solving

$$\mu(t)T = \int \mu(t)Q(t)\,dt$$

$$\exp(h_1t)T = \int \exp(h_1t)[h_2 + h_5 + h_3\cos(\alpha t + \beta) + h_4\cos^2(\alpha t + \beta)]\,dt$$

$$\exp(h_1t)T = \underbrace{(h_2 + h_5)\int \exp(h_1t)\,dt}_{1} + \underbrace{h_3\int \exp(h_1t)\cos(\alpha t + \beta)\,dt}_{2} + \underbrace{h_4\int \exp(h_1t)\cos^2(\alpha t + \beta)\,dt}_{3}. \quad \text{(A9)}$$

We can then solve the individual components of Eq. (A9) to give the estimated error. The solution of (1) is given by

$$\underbrace{(h_2 + h_5)\int \exp(h_1 t)\,dt}_{1} = \frac{h_2 + h_5}{h_1}\exp(h_1 t). \quad \text{(A10)}$$

Using integration by parts the solution of (2) is given by

$$\underbrace{h_3\int \exp(h_1 t)\cos(\alpha t + \beta)\,dt}_{2}$$

$$= \frac{h_3\alpha\exp(h_1 t)}{h_1^2 + \alpha^2}\left[\sin(\alpha t + \beta) + \frac{h_1}{\alpha}\cos(\alpha t + \beta)\right]. \quad \text{(A11)}$$

Similarly, using integration by parts the solution of (3) is given by

$$\underbrace{h_4\int \exp(h_1 t)\cos^2(\alpha t + \beta)\,dt}_{3}$$

$$= \frac{4\alpha^2 h_4}{h_1^2 + 4\alpha^2}\exp(h_1 t)\left[\frac{\sin(2\alpha t + 2\beta)}{4\alpha} + \frac{1}{2h_1} + \frac{h_1}{8\alpha^2}\cos(2\alpha t + 2\beta) + \frac{h_1}{8\alpha^2}\right]. \quad \text{(A12)}$$

Substituting (A10), (A11), and (A12) into (A9), and including a constant of integration (k_{int}), gives us

$$\begin{aligned}\exp(h_1 t)\Delta T &= \frac{h_2 + h_5}{h_1}\exp(h_1 t) \\ &+ \frac{h_3\alpha\exp(h_1 t)}{h_1^2 + \alpha^2}\left[\sin(\alpha t + \beta) + \frac{h_1}{\alpha}\cos(\alpha t + \beta)\right] \\ &+ \frac{4\alpha^2 h_4}{h_1^2 + 4\alpha^2}\exp(h_1 t)\left[\frac{\sin(2\alpha t + 2\beta)}{4\alpha} + \frac{1}{2h_1} + \frac{h_1}{8\alpha^2}\cos(2\alpha t + 2\beta) + \frac{h_1}{8\alpha^2}\right] \\ &+ k_{\text{int}}. \end{aligned} \quad \text{(A13)}$$

We can then rewrite (A13) as

$$\begin{aligned}(\Delta T_{\text{err}}) &= \frac{h_2 + h_5}{h_1} \\ &+ \frac{h_3\alpha}{h_1^2 + \alpha^2}\left[\sin(\alpha t + \beta) + \frac{h_1}{\alpha}\cos(\alpha t + \beta)\right] \\ &+ \frac{4\alpha^2 h_4}{h_1^2 + 4\alpha^2}\left[\frac{\cos(\alpha t + \beta)\sin(\alpha t + \beta)}{2\alpha} + \frac{h_1\cos^2(\alpha t + \beta)}{4\alpha^2} + \frac{1}{2h_1}\right] \\ &+ k_{\text{int}}\exp(-h_1 t). \end{aligned} \quad \text{(A14)}$$

d. The integrating factor k_{int}

In order to determine k_{int} (and hence the value of ΔT_{err}) we need to know the value of ΔT_{err} at a specified time. Replacing t with τ to represent a time interval, τ is then the time since ΔT_{err} was known. Heating errors due to solar radiation can persist after sunset but should have decayed to zero by the following sunrise. At sunrise the sensor environment will still be cooled by longwave radiation and the conductive and convective cooling will act to reduce the cooling effect of the longwave. If we assume the sensor environment is in equilibrium at sunrise [i.e., $d(\Delta T_{\text{err}})/dt = 0$], and that there is no solar radiation, Eq. (27) can be reduced to

$$\Delta T_{\text{err}} = \frac{h_5}{h_1}. \quad \text{(A15)}$$

Using this value of ΔT_{err} at sunrise [substituting Eq. (A15) into the lhs of Eq. (27)], letting ϕ_{sr} = the hour angle at sunrise and with $\tau = 0$, we can solve Eq. (27) at sunrise and k_{int} becomes

$$\begin{aligned}k_{\text{int}} = -\Bigg\{&\frac{h_2}{h_1} + \frac{4\alpha^2 h_4}{4\alpha^2 + h_1^2}\left[\frac{\cos(\phi_{\text{sr}})\sin(\phi_{\text{sr}})}{2\alpha} + \frac{h_1\cos^2(\phi_{\text{sr}})}{4\alpha^2} + \frac{1}{2h_1}\right] \\ &+ \frac{\alpha h_3}{\alpha^2 + h_1^2}\left[\sin(\phi_{\text{sr}}) + \frac{h_1}{\alpha}\cos(\phi_{\text{sr}})\right]\Bigg\}. \end{aligned} \quad \text{(A16)}$$

APPENDIX B

List of Symbols

Symbol	Name
α	$-(\pi/12)$
A_c	Surface area of the sensor environment in contact with the atmosphere (m^2)
a_i	Coefficient from okta model [i = cloud cover (oktas)]
A_{LW}	Surface area of sensor environment (m^2)

a_{lw}	Empirical coefficient from downwelling longwave radiation model of Josey et al. (2003)
A_s	Area normal to the solar radiation (m^2)
a_s	Solar absorptivity of sensor environment
$\alpha t + \beta$	hour angle (rad)
b_i	Coefficient from okta model [i = cloud cover (oktas)]
b_{lw}	Empirical coefficient from downwelling longwave radiation model of Josey et al. (2003)
c	Specific heat capacity of sensor environment J kg^{-1} K^{-1}
c_1	Constant
c_2	Constant
c_{lw}	Empirical coefficient from downwelling longwave radiation model of Josey et al. (2003)
D	Difference between dewpoint temperature and air temperature (K)
δ	Characteristic length (m)
day	Day of year
dr	$\pi/180$
ΔT_{eff}	Temperature adjustment to give effective blackbody air temperature (K)
ΔT_{err}	Heating error (K)
ε_{LW}	Thermal emissivity
ϕ	Hour angle (rad)
ϕ_t	Hour angle at time t (rad)
h_μ	Convective heat transfer coefficient (W m^{-2} K^{-1})
h_o	Conductive heat transfer coefficient (W m^{-2} K^{-1})
i	Total cloud cover (oktas)
k	Thermal conductivity of air (W m^{-1} K^{-1})
lat	Latitude (°N)
lon	Longitude (°E)
m	Mass of sensor environment (kg)
ν	Kinematic viscosity of air (m^2 s^{-1})
n	Fractional cloud cover
Nu	Nusselt number
Pr	Prandtl number
Q_{COND}	Rate of energy transfer between the ship and atmosphere through conduction (W)
Q_{CONV}	Rate of energy transfer between the ship and atmosphere through convection (W)
Q_{LW}	Net rate of thermal heating and cooling (W)
Q_{LW_ATMOS}	Rate of atmospheric downwelling longwave radiation absorbed (W)
Q_{LW_SHIP}	Rate of heat loss due to radiative cooling (W)
Q_{ship}	Energy stored by sensor environment and sensors (J)
Q_{SW}	Rate of solar energy absorbed (W)
Re	Reynolds number
R_{LW}	Atmospheric downwelling longwave radiation (W m^{-2})
R_s	Incident solar radiation (W m^{-2})
R_{top}	Solar radiation at top of atmosphere (1368) (W m^{-2})
$\sin\theta$	Sine of solar elevation
σ_{SB}	Stefan–Boltzmann constant (5.67×10^{-8}) (W m^{-2} K^{-4})
t	Time (s)
τ	Time since sunrise (s)
T_{air}	Air temperature (K)
T_{dew}	Dewpoint temperature (K)
T_{eff}	Effective blackbody temperature of the atmosphere (K)
T_{ship}	Temperature of sensor environment (K)
τ_{ss}	Time since sunset (s)
utc	Hour (UTC)
V	Relative wind speed (m s^{-1})

REFERENCES

Anderson, S. P., and M. F. Baumgartner, 1998: Radiative heating errors in naturally ventilated air temperature measurements made from buoys. *J. Atmos. Oceanic Technol.,* **15,** 157–173.

Birch, K. G., and R. W. Pascal, 1987: A meteorological system for research applications—MultiMet. *Proc. Fifth Int. Conf. on Electronics for Ocean Technology*, Edinburgh, United Kingdom, Institute of Electronic and Radio Engineers, IERE Publication 72, 7–12.

Çengel, Y. A., 1998: *Heat Transfer: A Practical Approach.* McGraw-Hill, 1024 pp.

Chapman, A. J., 1984: *Heat Transfer*. Collier Macmillan, 608 pp.

Chenoweth, M., 2000: A new methodology for homogenization of 19th century marine air temperature data. *J. Geophys. Res.,* **105,** 29 145–29 154.

da Silva, A. M., C. C. Young, and S. Levitus, 1994: *Algorithms and Procedures.* Vol. 1, *Atlas of Surface Marine Data*, *Algorithms and Procedures*, NOAA Atlas NESDIS 6, 83 pp.

Deitrich, G., 1950: Systematic errors in the observe surface water and air temperature at sea and their effect on the determination of heat exchange between the sea and atmosphere. *Dtsch. Hydrogr. Z.,* **3,** 314–324.

Diaz, H. F., C. K. Folland, T. Manabe, D. E. Parker, R. W. Reynolds, and S. D. Woodruff, 2002: Workshop on advances in the use of historical marine climate data. *WMO Bull.,* **51,** 377–380.

Dobson, F. W., and S. D. Smith, 1988: Bulk models of solar radiation at sea. *Quart. J. Roy. Meteor. Soc.,* **114,** 165–182.

Folland, C. K., 1971: Daytime temperature measurements on weather ship 'Weather Reporter.' *Meteor. Mag.,* **100,** 6–14.

——, D. E. Parker, and F. E. Yates, 1984: Worldwide marine air temperature fluctuations 1856–1981. *Nature,* **310,** 670–673.

Fu, C., H. F. Diaz, D. Dong, and J. O. Fletcher, 1999: Changes in atmospheric circulation over Northern Hemisphere oceans associated with the rapid warming of the 1920s. *Int. J. Climatol.,* **19,** 581–606.

Glahn, W., 1933: False measurements of air temperatures on ships. *Der Seewart,* **2,** 250–256.

Goerss, J. S., and C. E. Duchon, 1980: Effect of ship heating on dry-bulb temperature measurements in GATE. *J. Phys. Oceanogr.,* **10,** 478–479.

Hayashi, S., 1974: Some problems in marine meteorological observations, particularly of pressure and temperature. *J. Meteor. Res.,* **26,** 84–87.

Josey, S. A., D. Oakley, and R. W. Pascal, 1997: On estimating the atmospheric longwave flux at the ocean surface from ship meteorological reports. *J. Geophys. Res.,* **102,** 27 961–27 972.

——, E. C. Kent, and P. K. Taylor, 1999: New insights into the ocean

heat budget closure problem from analysis of the SOC air–sea flux climatology. *J. Climate,* **12,** 2856–2880.

——, ——, and B. Sinha, 2001: Can a state of the art atmospheric general circulation model reproduce recent NAO related variability at the air–sea interface? *Geophys. Res. Lett.,* **28,** 4543–4546.

——, R. W. Pascal, P. K. Taylor, and M. J. Yelland, 2003: A new formula for determining the atmospheric longwave flux at the ocean surface at mid-high latitudes. *J. Geophys. Res.,* **108,** 3108, doi:10.1029/2002JC001418.

Kent, E. C., and P. K. Taylor, 1996: Accuracy of humidity measurements on ships: Consideration of solar radiation effects. *J. Atmos. Oceanic Technol.,* **13,** 1317–1321.

——, ——, B. S. Truscott, and J. S. Hopkins, 1993a: The accuracy of voluntary observing ships' meteorological observations—Results of the VSOP-NA. *J. Atmos. Oceanic Technol.,* **10,** 591–608.

——, R. J. Tiddy, and P. K. Taylor, 1993b: Correction of the marine air temperature observations for solar radiation effects. *J. Atmos. Oceanic Technol.,* **10,** 900–906.

Monteith, J. L., 1957: Dew. *Quart. J. Roy. Meteor. Soc.,* **83,** 322–341.

NAG, cited 2002: The NAG Fortran Library Manual, Mark 20. The Numerical Algorithms Group Ltd. [Available online at: http://www.nag.co.uk/numeric/fl/manual/html/FLlibrarymanual.asp.]

Parker, D. E., P. D. Jones, C. K. Folland, and A. Bevan, 1994: Interdecadal changes of surface temperature since the late 19th century. *J. Geophys. Res.,* **99,** 14 373–14 399.

Rayner, N. A., D. E. Parker, E. B. Horton, C. K. Folland, L. V. Alexander, D. P. Rowell, E. C. Kent, and A. Kaplan, 2003: Global analyses of SST, sea ice and night marine air temperature since the late 19th century. *J. Geophys. Res.,* **108,** 4407, doi:10.1029/2002JD002670.

Reynolds, R. W., and T. M. Smith, 1994: Improved global sea surface temperature analyses using optimum interpolation. *J. Climate,* **7,** 929–948.

Smith, T. M., and R. W. Reynolds, 2002: Bias corrections for historical sea surface temperature based on marine air temperatures. *J. Climate,* **15,** 73–87.

Taylor, P. K., M. J. Yelland, C. G. Davies, and R. J. Tiddy, 1992: Meteorological observations on the OWS *Cumulus*—Status and quality of the data set. James Rennell Centre Internal Rep. 6, 21 pp.

——, and WCRP/SCOR Working Group on Air-Sea Fluxes, 2000: Intercomparison and validation of ocean–atmosphere energy flux fields (November 2000). WMO/TD No. 1036, 306 pp.

Trenberth, K. E., J. R. Christy, and J. W. Hurrell, 1992: Monitoring global monthly mean surface temperatures. *J. Climate,* **5,** 1405–1423.

Woodruff, S. D., H. F. Diaz, J. D. Elms, and S. J. Worley, 1998: COADS release 2 data and metadata enhancements for improvements of marine surface flux fields. *Phys. Chem. Earth,* **23,** 517–527.